

# Potential anomalies on a sphere: Applications to the thickness of the lunar crust

Mark A. Wieczorek, and Roger J. Phillips

Department of Earth and Planetary Sciences, Washington University, St. Louis, Missouri

**Abstract.** A new technique for calculating potential anomalies on a sphere due to finite amplitude relief has been developed. We show that by raising the topography to the  $n$ th power and expanding this field into spherical harmonics, potential anomalies due to topography on spherical density interfaces can be computed to arbitrary precision. Using a filter for downward continuing the Bouguer anomaly, we have computed a variety of crustal thickness maps for the Moon, assuming both a homogeneous as well as a dual-layered crust. The crustal thickness maps for the homogeneous model give plausible results, but this model is not consistent with the seismic data, petrologic evidence, and geoid to topography ratios, all of which suggest some form of crustal stratification. Several dual-layered models were investigated, and it was found that only models with both upper and lower crustal thickness variations could satisfy the gravity and topography data. These models predict that the entire upper crust has been excavated beneath the major nearside multiring basins. Additionally, significant amounts of lower crustal material was excavated from these basins, especially beneath Crisium. This model also predicts that mantle material should not have been excavated during the South-Pole Aitken basin forming event, and that lower crustal material should be exposed at the surface in this basin.

## 1. Introduction

The thickness of the lunar crust has been a subject of debate since the Apollo missions. It was quickly realized that both the lunar gravity and topography were primarily controlled by the large impact basins and mare flows that subsequently filled many of these circular depressions. Using Apollo data, there were several efforts to map the global crustal thickness of the Moon [Bills and Ferrari, 1977; Thurber and Solomon, 1978; Bratt *et al.*, 1985], but these studies were thwarted by the low resolution and limited coverage of the lunar gravity and topographic data sets. These studies were also hindered by a limited knowledge of the thickness of the mare basalt flows, which are presumably denser than the underlying crust. Consequently, either the gravitational attraction due to the mare was ignored or the unknown thickness of the mare was modeled using a pre-mare isostatic assumption. These studies also assumed implicitly that the lunar gravity field could be explained exclusively in terms of surface topography, surface basalt flows, and relief along the lunar Moho (which lies 60 km beneath the Apollo 12 and 14 sites [Toksöz *et al.*, 1974]).

In 1994, the Clementine mission to the Moon [Nozette *et al.*, 1994] obtained new lunar gravity data [Lemoine *et al.*, 1997] and near global topography data [Smith *et al.*, 1997]. Using these data sets, Zuber *et al.* [1994] and Neumann *et al.* [1996] computed a global crustal thickness map assuming that the crust was uniform in composition. Neumann *et al.* [1996] also noted that the traditional first-order method of treating finite amplitude topography as two-dimensional infinitesimal surface densities was not entirely appropriate, given that the crustal thicknesses varied dramatically across the surface ( $\sim 20$  to 120 km). In order to rectify this problem, the higher-order Cartesian algorithm of

Parker [1972] was used to invert for crustal structure beneath the major impact basins. Downward continuation of the Bouguer correction was also stabilized by using a filter which minimized the slope and curvature of the lunar Moho [Phipps Morgan and Blackman, 1993]. It was shown that if one were only to use the first-order theory (in which topography is approximated by a surface density), then crustal thickness estimates beneath the basins would be grossly underestimated (of the order of 10 to 20 km) when compared to the results of the higher-order theory.

In this study we develop a new method for computing potential anomalies on a sphere due to finite amplitude topography. We show that by raising the topography to the  $n$ th power and expanding this field into spherical harmonics, potential anomalies due to topography on a spherical density interface can easily be computed to arbitrary precision. This methodology is the spherical analog to the Cartesian result of Parker [1972]. We additionally derive a smoothing filter to be used when downward continuing gravity anomalies on a sphere.

Using these techniques, we set forth to map the crustal thickness variations across the lunar surface. All previous models have assumed that the crust is uniform in composition and that compensation occurs at the lunar Moho, the depth of which has been seismically constrained at one locale. There is considerable evidence, however, that suggests that this view is not entirely correct and that the lunar crust is stratified in some sense: (1) The existence of a sharp seismic discontinuity 20 km below the Apollo 12 and 14 sites is hard to explain without invoking some form of compositional change [Toksöz *et al.*, 1974]. (2) The noritic low-K Fra Mauro (LKFM) impact melts have commonly been attributed to a lower crustal origin [Ryder and Wood, 1977; Charette *et al.*, 1977]. (3) The composition of basin ejecta blankets becomes increasingly more mafic with increasing basin size [Spudis *et al.*, 1984, 1996]. (4) The geoid to topography ratios for the nearside lunar highlands are most consistent with the crust being stratified, rather than being homogeneous [Wieczorek and Phillips, 1997].

Copyright 1998 by the American Geophysical Union.

Paper number 97JE03136.  
0148-0227/98/97JE-03136\$09.00

In the present study we have also used improved estimates of the mare thickness for the nearside basins derived from Clementine altimetry data [Williams and Zuber, 1996]. These estimates, in general, are considerably less than those of Solomon and Head [1980], which were used in the analysis of Neumann *et al.* [1996].

A variety of single- and dual-layered crustal models were used to explain the observed lunar gravity and topographic data. A uniform composition crust with compensation occurring entirely at the Moho was found to give plausible results (i.e., the crustal thickness was everywhere nonnegative), but as we noted above, this model is not consistent with the petrological and geophysical data. A model with upper crustal anorthositic material being compensated entirely at the intracrustal interface was also considered. This model, however, yielded negative upper crustal thicknesses beneath the basins and was therefore unphysical for large portions of the lunar surface. A dual-layered model in which the lower crust was constrained to have a constant thickness was also investigated. Though this model proved to be a substantial improvement over the single-layered intracrustal compensation model, this model also yielded unphysical results beneath the larger basins.

The only dual-layered model investigated that gave plausible crustal thicknesses over the entire lunar surface was one in which both the upper and lower crustal layers were allowed to vary in thickness. The results of this model imply that the entire upper crust was excavated during the major nearside basin-forming events. Additionally, a significant amount of lower crustal material was also excavated during many of these events. Though one may have expected the South-Pole Aitken basin-forming event to have excavated mantle material, our results suggest that the basin floor should be composed entirely of lower crustal material with an average thickness of about 40 km.

## 2. Theory

In this section we develop the theoretical aspects of constructing global crustal thickness models for a planet. This encompasses (1) developing a method of computing potential anomalies due to finite amplitude relief on a sphere and (2) developing a stabilizing filter to be used when downward continuing gravity anomalies on a sphere. In section 3 we use these methods to compute both single- and dual-layered crustal thickness models for the Moon, and in section 4 we discuss some of the more significant features of these models.

### 2.1. Potential Anomalies on a Sphere

The interior structure of a planet can be constrained with a knowledge of the planet's gravitational potential and surface topography. Since inverse models of the gravity field are nonunique, potential anomalies have traditionally been interpreted as being due to relief along a small number of density interfaces within the planet. When the relief along these surfaces is small in comparison to the size of the region being investigated, a first-order treatment of the relationship between this relief and the corresponding potential anomaly is usually adequate. In this approach, one assumes that the finite amplitude relief can be modeled as a two-dimensional surface density, and then the harmonic coefficients (either Fourier or spherical) of the topography are found to be linearly related to the potential coefficients [e.g., Dorman and Lewis, 1970].

When the relief along a density interface becomes large, these first-order approximations break down. Though one could in principle integrate the mass distribution to determine the potential anomaly at a specific location, this is in general very time con-

suming and difficult to invert for model parameters. Alternatively, Parker [1972] has shown in Cartesian space that the Fourier transform of the potential due to finite amplitude relief along a density interface is given exactly by the infinite sum

$$\mathcal{F}[U(\mathbf{r})] = 2\pi \Delta\rho G e^{-|\mathbf{k}|z_0} \sum_{n=1}^{\infty} \frac{|\mathbf{k}|^{n-2}}{n!} \mathcal{F}[H^n(\mathbf{r})] \quad (1)$$

where the operator  $\mathcal{F}$  is the Fourier transform,  $\mathbf{r}$  is the position vector,  $k$  is the wavenumber,  $G$  is the gravitational constant,  $\Delta\rho$  is the density contrast,  $z_0$  is the depth of this interface from the observation plane, and  $H^n$  is the topography raised to the  $n$ th power. Using this formula, potential anomalies can be quickly computed to arbitrary precision using the fast Fourier transform (FFT).

Given that the algorithm of Parker [1972] is only valid in Cartesian space, we have developed an analogous formalism for use on a sphere. We start with Newton's law of gravitation

$$U(\mathbf{r}, \theta, \phi) = \int_M \frac{G dm'}{|\mathbf{r} - \mathbf{r}'|} \quad (2)$$

and the identity

$$\frac{1}{|\mathbf{r} - \mathbf{r}'|} = \frac{1}{r} \sum_{l=0}^{\infty} \left(\frac{r'}{r}\right)^l P_l(\cos \gamma) \quad r > r' \quad (3)$$

where  $\mathbf{r}$  and  $\mathbf{r}'$  are any pair of radius vectors,  $\gamma$  is the angle subtended between these two vectors, and  $P_l$  is the Legendre polynomial of degree  $l$ . Using the spherical harmonic addition formula [e.g., Lambeck, 1988], the Legendre polynomials can be expanded as

$$P_l(\cos \gamma) = \frac{1}{(2l+1)} \sum_{m=0}^l \sum_{i=1}^2 Y_{ilm}(\theta, \phi) Y_{ilm}(\theta', \phi') \quad (4)$$

where  $Y_{ilm}$  is the spherical harmonic function of degree  $l$  and order  $m$  normalized to  $4\pi$

$$\int_{\Omega} Y_{ilm}(\theta, \phi) Y_{i'l'm'}(\theta, \phi) d\Omega = \delta_{ii'} \delta_{ll'} \delta_{mm'} 4\pi \quad (5)$$

where  $\delta_{ll'}$  is the Kronecker delta,  $d\Omega = \sin \theta d\theta d\phi$ , and  $\theta$  and  $\phi$  are colatitude and longitude, respectively.

Considering only topography  $H(\theta, \phi)$  referenced to a radius  $D$  with density contrast  $\Delta\rho$ , substituting the above identities into Newton's law of gravitation and integrating with respect to  $r$  yields

$$U(\mathbf{r}, \theta, \phi) = \frac{G \Delta\rho}{r} \sum_{ilm} \frac{Y_{ilm}(\theta, \phi)}{r^l (2l+1)(l+3)} \times \int_{\Omega'} Y_{ilm}(\theta', \phi') r'^{l+3} \Big|_D^{D+H(\theta', \phi')} d\Omega' \quad (6)$$

for all  $r > D + \max(H)$ . Next, we expand the last term in the above integral using the binomial theorem

$$[D + H(\theta', \phi')]^{l+3} = D^{l+3} + D^{l+3} \sum_{n=1}^{l+3} \frac{H^n(\theta', \phi')}{D^n n!} \prod_{j=1}^n (l+4-j) \quad (7)$$

and expand the powers of topography  $H^n$  into spherical harmonics

$$H^n(\theta', \phi') = \sum_{i'l'm'} n_{h_{i'l'm'}} Y_{i'l'm'}(\theta', \phi'). \quad (8)$$

Inserting the above two equations into (6), utilizing the orthogonal properties of the spherical harmonic functions, and simplifying yields

$$U(r, \theta, \phi) = \frac{GM}{r} \sum_{ilm} \left(\frac{D}{r}\right)^l C_{ilm}^+ Y_{ilm}(\theta, \phi) \quad (9)$$

where

$$C_{ilm}^+ = \frac{4\pi \Delta \rho D^3}{M(2l+1)} \sum_{n=1}^{l+3} \frac{n_{h_{ilm}}}{D^n n!} \frac{\prod_{j=1}^n (l+4-j)}{(l+3)}. \quad (10)$$

Using the same technique, it can also be shown that for all  $r < D + \min(H)$

$$U(r, \theta, \phi) = \frac{GM}{r} \sum_{ilm} \left(\frac{r}{D}\right)^{l+1} C_{ilm}^- Y_{ilm}(\theta, \phi) \quad (11)$$

where

$$C_{ilm}^- = \frac{4\pi \Delta \rho D^3}{M(2l+1)} \sum_{n=1}^{\infty} \frac{n_{h_{ilm}}}{D^n n!} \frac{\prod_{j=1}^n (l+j-3)}{(l-2)}. \quad (12)$$

Equation (10) is analogous to that of (1), except that instead of taking successive Fourier transforms of powers of the topography, powers of topography are expanded into spherical harmonics. We note that in spherical coordinates the potential coefficients exterior to a mass distribution can be computed exactly by this finite sum. This is in contrast to the algorithm of Parker [1972] in which the potential coefficients are expressed in terms of an infinite sum. Though the process of computing spherical harmonic coefficients of a field is not as rapid as taking FFTs, this method does not suffer from the Cartesian geometry which is implicit in the formalism of Parker [1972]. Additionally, it is straightforward to show that the magnitude of each successive term in (10) and (12) is smaller than the previous term. Therefore, in practice, these sums can be truncated after a given precision has been achieved.

As shown above, the problem of computing potential anomalies reduces to computing the spherical harmonic expansion of the topography raised to a given power. Though this is most easily achieved by numerical integrations or least squares fitting, we note that an exact analytic solution does exist. We start by expressing the topographic field in complex form [e.g., Kaula, 1967]

$$H(\theta, \phi) = \sum_{lm} h_{lm} Y_{lm}(\theta, \phi) \quad (13)$$

and expand the topography to the  $n$ th power in spherical harmonics as

$$n_{h_{ilm}} = \frac{1}{4\pi} \int_{\Omega} H^{n-1}(\theta, \phi) H(\theta, \phi) Y_{lm}^*(\theta, \phi) d\Omega \quad (14)$$

where  $Y_{lm}^*$  is the complex conjugate of the spherical harmonic function. Expanding  $H^n$  and  $H^{n-1}$  in (14) results in

$$n_{h_{ilm}} = \frac{1}{4\pi} \sum_{l_1 m_1} \sum_{l_2 m_2}^{n-1} h_{l_1 m_1} h_{l_2 m_2} \times \int_{\Omega} Y_{l_1 m_1}(\theta, \phi) Y_{l_2 m_2}(\theta, \phi) Y_{lm}^*(\theta, \phi) d\Omega \quad (15)$$

or

$$n_{h_{ilm}} = \sum_{l_1 m_1} \sum_{l_2 m_2}^{n-1} h_{l_1 m_1} h_{l_2 m_2} \times \sqrt{\frac{(2l_1+1)(2l_2+1)}{(2l+1)}} C_{l_1 0 l_2 0}^{l 0} C_{l_1 m_1 l_2 m_2}^{lm} \quad (16)$$

where  $C_{l_1 m_1 l_2 m_2}^{lm}$  are the Clebsch-Gordon coefficient [e.g., Varshalovich *et al.*, 1988].

The results in this section were partially anticipated by previous researchers. A special case of (10) involving global isostasy was presented by Rapp [1989]. Additionally, Balmino [1994] presented a result equivalent to (10) and derived a more complex form of (16).

## 2.2. Determination of Subsurface Relief: Downward Continuation of Potential Anomalies

If global topography for a planet is known, the above method can be used to determine the Bouguer correction (the gravitational contribution from the topography) and Bouguer anomaly (the total gravity field minus the Bouguer correction). The Bouguer anomaly can then be used to infer relief along a hypothetical density interface below the surface. In doing this though, the Bouguer anomaly needs to be downward continued to this interface, and this process amplifies noise in the data.

Phipps Morgan and Blackman [1993] addressed this problem in Cartesian space using an inverse approach. They set forth to determine the hypothetical relief along an interface which (1) minimized the misfit between the observed and modeled gravitational field and (2) minimized the slope and curvature along this interface. A simple downward continuation filter was derived that contained two adjustable parameters which controlled the amount of minimization of the slope and curvature, respectively.

Since Phipps Morgan and Blackman [1993] only considered Cartesian geometry, we derive a downward continuation filter to be used in spherical coordinates. Instead of minimizing the slope and curvature of the model solution, we only attempt to minimize the total relief along this surface on a degree by degree basis. Though this approach may not appear to be as robust as that of Phipps Morgan and Blackman [1993], we show that it is numerically indistinguishable from their minimum slope solution.

We start by constructing the function

$$\Phi = \left[ C_{ilm}^{BA} - C_{ilm}^D \left(\frac{D}{R}\right)^l \right]^2 + \lambda (h_{ilm})^2 \quad (17)$$

which is a combined measure of the potential misfit and topographic relief. In this expression,  $C_{ilm}^{BA}$  are the Bouguer anomaly coefficients,  $C_{ilm}^D$  are the potential coefficients due to relief  $h_{ilm}$  along an interface referenced to radius  $D$ , and  $\lambda$  is a Lagrange multiplier.

Substituting in (10) for  $C_{ilm}^D$ , minimizing this function with respect to  $h_{ilm}$ , and ignoring higher-order terms yields

$$h_{ilm} = w_l \left[ \frac{C_{ilm}^{BA} M (2l+1) \left(\frac{R}{D}\right)^l}{4\pi \Delta\rho D^2} - \frac{D \sum_{n=2}^{l+3} \frac{h_{ilm}}{D^n n!} \prod_{j=1}^n (l+4-j)}{(l+3)} \right] \quad (18)$$

where

$$w_l = \left\{ 1 + \lambda \left[ \frac{M (2l+1) \left(\frac{R}{D}\right)^l}{4\pi \Delta\rho D^2} \right]^2 \right\}^{-1} \quad (19)$$

is the downward continuation filter. The last term in (18) is the higher-order correction that takes into account the finite amplitude nature of relief along this interface. Since each successive term in this sum is decreased in magnitude, this sum can be truncated after the correction terms become smaller than the measurement error in the Bouguer anomaly. Equations (18) and (19) can then be used to iteratively determine the hypothetical relief along a subsurface density interface. This spherical algorithm is analogous to the Cartesian algorithm of *Parker and Huestis* [1974] and *Oldenburg* [1974].

The Lagrange multiplier  $\lambda$  determines how much the relief will be minimized. Clearly, if  $\lambda = 0$ , then the relief is not filtered at all, whereas the larger the value of  $\lambda$ , the more the short-wavelength topography will be filtered. Choosing a value for  $\lambda$  is a subjective process, and we use the power spectrum of the potential coefficients and their associated errors as an appropriate guide. In this study, we choose  $\lambda$  such that  $w_l = 0.5$  for the degree where the power of the error spectrum of the potential field equals the power of the potential spectrum. For the Moon, this occurs at degree 30.

Figure 1 shows a plot of the downward continuation filter as a function of spherical harmonic degree, where the filter is constrained to be 0.5 at degree 30. Also plotted are the two end-members (minimum slope and minimum curvature) of the *Phipps Morgan and Blackman* [1993] filter where the Cartesian wavenumber  $k$  has been replaced by the spherical approximation  $l/R$ . As can be seen, the spectral response of (19) is nearly indistinguishable from the Cartesian minimum slope filter.

### 3. Lunar Crustal Thickness Models

In this section we use the above technique to constrain the thickness of the lunar crust. It will be assumed that the lunar gravitational perturbations are due to surface topography and surface basalt flows, as well as intracrustal and/or Moho relief.

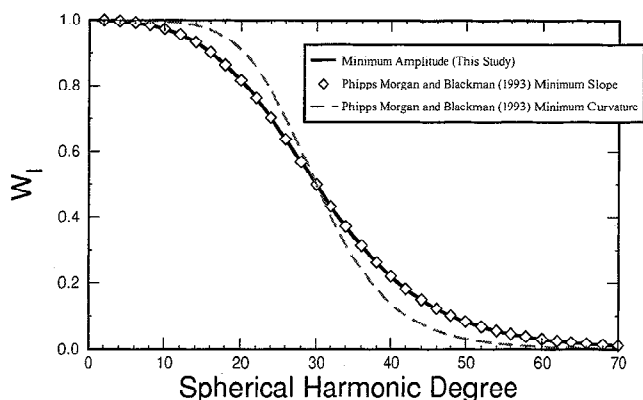


**Figure 1.** Plot of the downward continuation filter as a function of degree, where the filter is constrained to be 0.5 at degree 30.

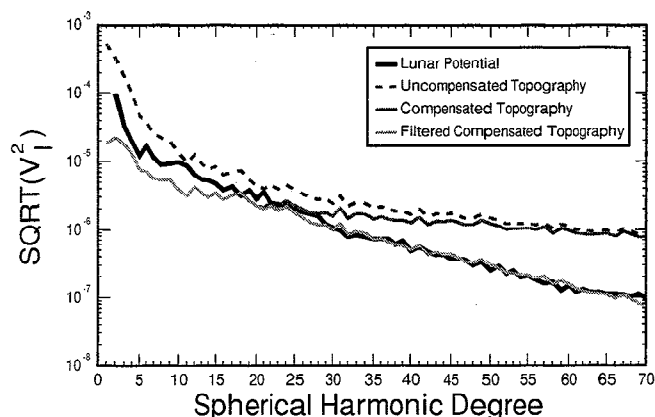


**Figure 2.** Square root of the power spectrum as a function of spherical harmonic degree, with  $\rho_c = 2900 \text{ kg/m}^3$  and  $\rho_m = 3400 \text{ kg/m}^3$ .

The first step of the present analysis is to compute the complete Bouguer correction which is due to the surface relief and surface basalt flows. In taking into account the gravitational attraction of surface basalt flows, we only considered the circular mare which reside within the large multiring basins. The irregular mare are generally inferred to be thin (approximately 0.5 km [*DeHon and Waskom*, 1976; *DeHon*, 1979]) and should not have a considerable effect on the Bouguer correction, nor the subsequent crustal thickness determinations. Our primary source to the thickness of the circular mare is the disk model of *Solomon and Head* [1980]. Their study, however, attempted to explain the magnitude of the "mascons" (positive gravity anomalies associated with some basins) exclusively as superisostatic surface basalt flows and did not take into account possible nonisostatic Moho relief and/or flexure of the lithosphere. Additionally, the gravity model that was used in their study possessed significant uncertainties.

Using newly obtained Clementine altimetry data, *Williams and Zuber* [1996] have been able to constrain the maximum basalt fill for the nearside basins by reanalyzing the depth-diameter relationship of large lunar basins. They have found that the maximum basalt fill is generally considerably less than was inferred in the model of *Solomon and Head* [1980]. For instance, the maximum thickness of basalt flows in the Imbrium basin was found to be just under 6 km, as opposed to 10 km from the model of *Solomon and Head* [1980]. In this study we have used the disk model of *Solomon and Head* [1980] constrained by the revised maximum

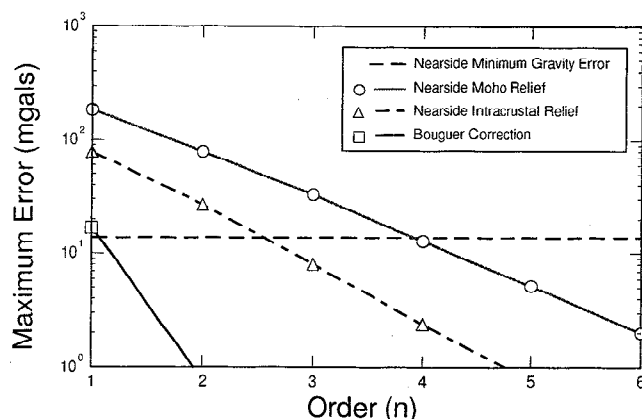


**Figure 3.** Maximum error associated with truncating (10) at order  $n$  when compared to the  $n = 10$  solution.



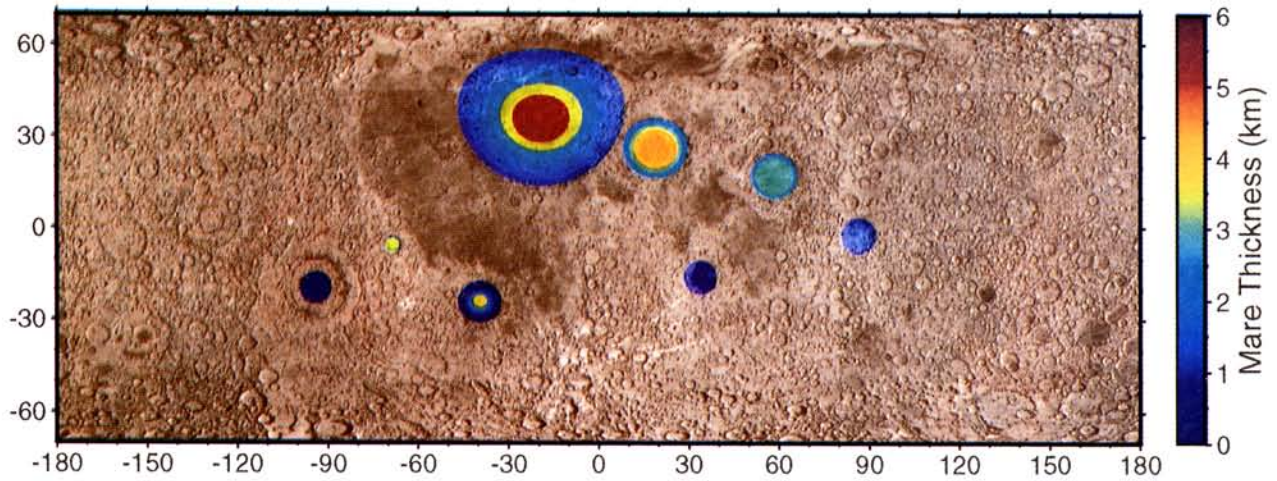


**Plate 1.** Basalt thickness model of *Solomon and Head* [1980] constrained by the revised maximum thicknesses of *Williams and Zuber* [1996].

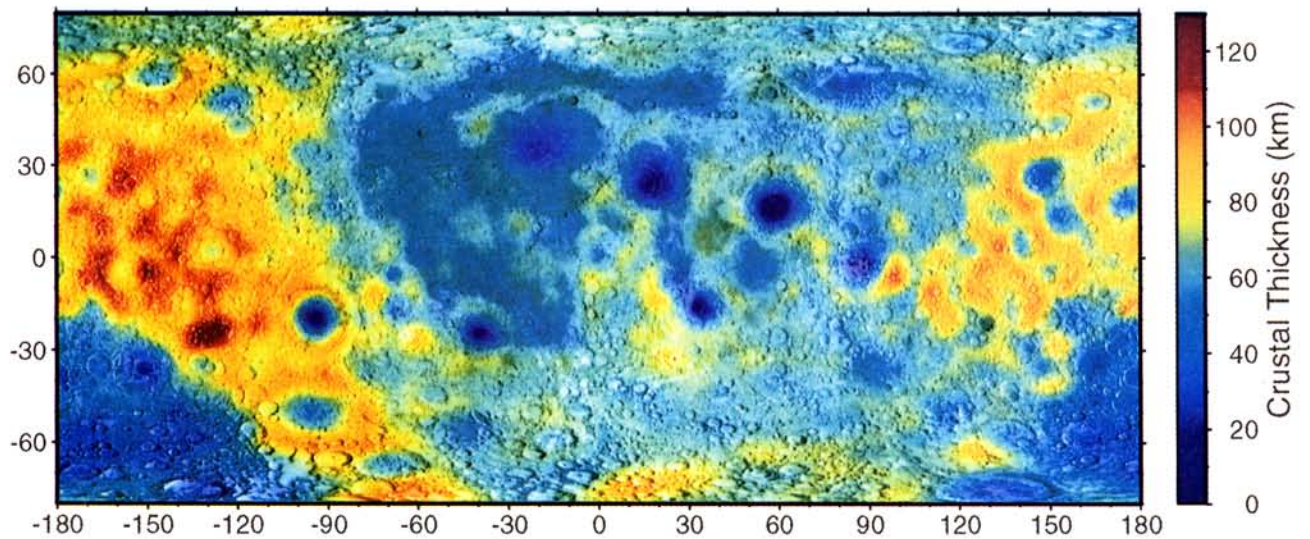


**Plate 2.** Crustal thickness minus mare fill for a uniform density crust with compensation occurring at the seismically determined Moho.

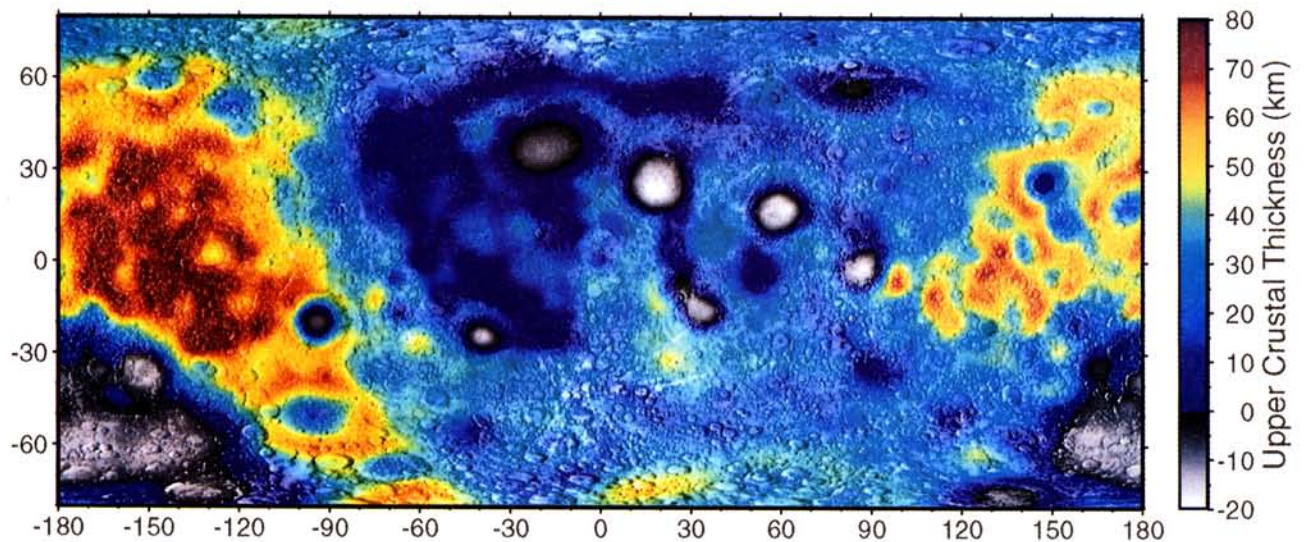


**Plate 3.** Upper crustal thickness minus mare fill for an anorthositic upper crust compensated entirely at an intracrustal density interface.



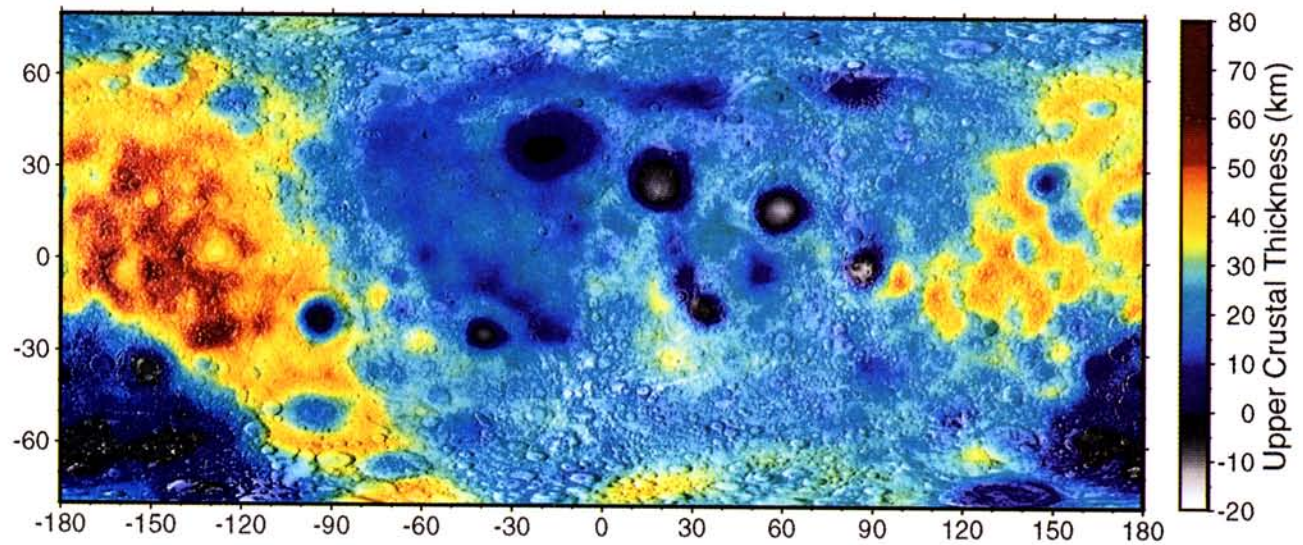


**Plate 4.** Upper crustal thickness minus mare fill for a dual-layered model with a constant thickness lower crust.

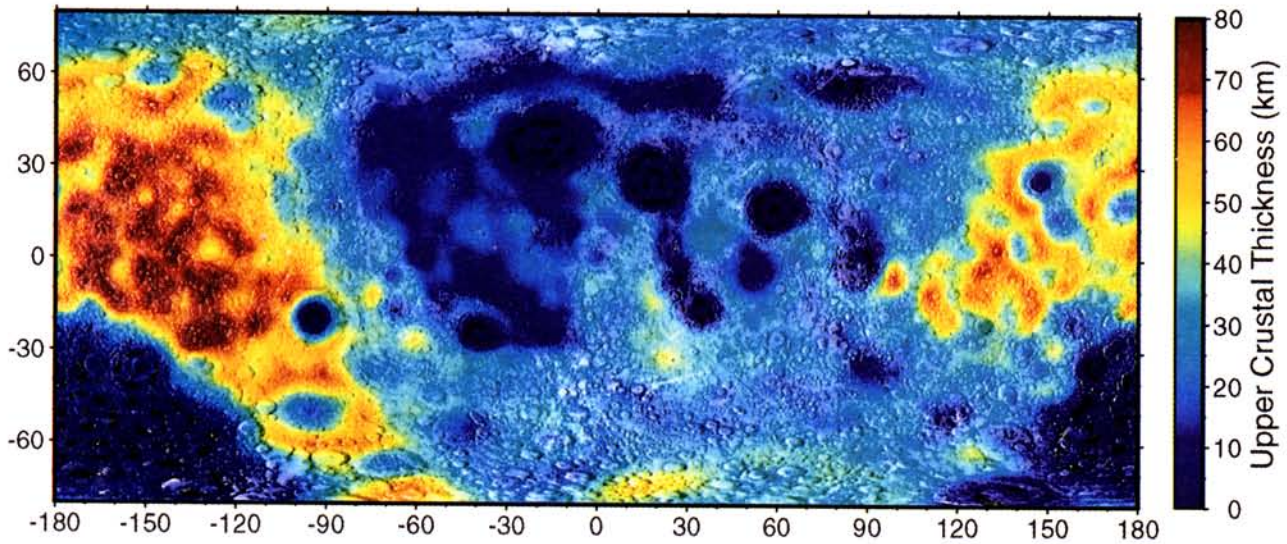


**Plate 5.** Upper crustal thickness minus mare fill for the dual-layered model with both upper and lower crustal thickness variations.

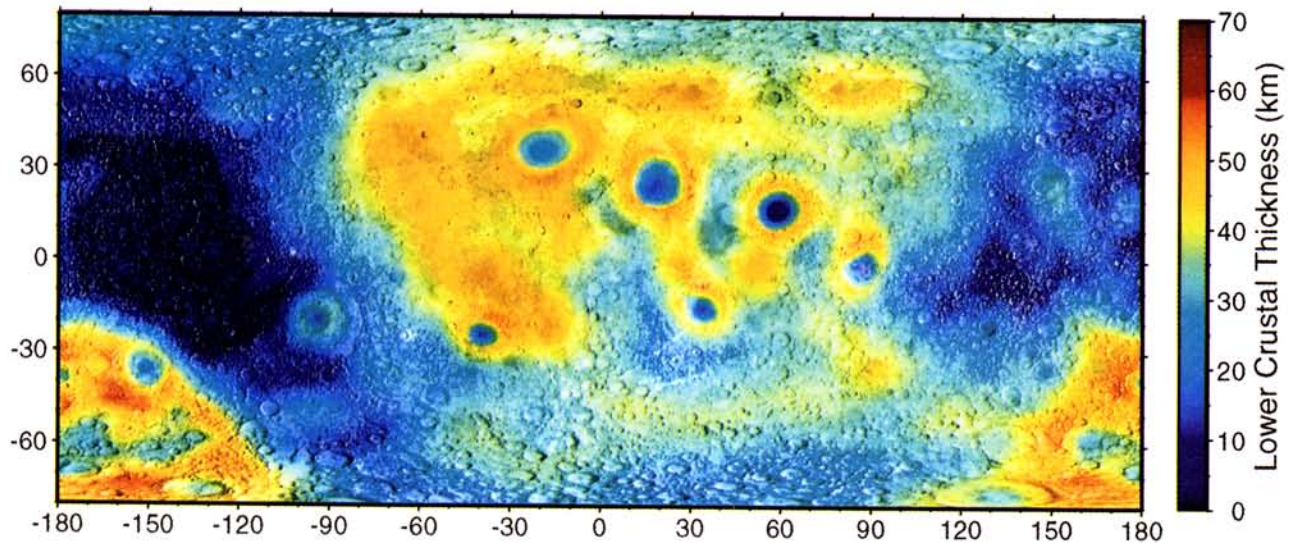


**Plate 6.** Lower crustal thickness for the dual-layered model with both upper and lower crustal thickness variations.



thicknesses from K. K. Williams and M. T. Zuber (Measurement and analysis of lunar basin depths from Clementine altimetry, manuscript in preparation, 1997) (see Plate 1). In the following models, we use a basalt density of  $\rho_{\text{mare}} = 3300 \text{ kg/m}^3$ .

As was noted by Neumann *et al.* [1996], the Bouguer correction has substantial short-wavelength power which is not resolvable in the current lunar gravity model (GLGM-2), and hence needs to be filtered in some sense before the Bouguer anomaly is computed. This is illustrated in Figure 2. Plotted in this figure are the root power spectrum of the observed lunar potential, the first-order Bouguer correction due to topography alone, and the root power spectrum assuming that the topography is perfectly compensated by an Airy mechanism at 60 km depth. As can be seen, both the uncompensated topography and Airy-compensated models have substantially more short-wavelength power than the observed lunar spectrum. This is most likely an artifact of using an a priori power law (Kaula's rule) to limit the short-wavelength gravitational power when computing the gravity field [Lemoine *et al.*, 1997]. We corrected for this effect by applying the posteriori filter to the Bouguer correction

$$f_l = \left( \frac{R}{1820} \right)^l \left( \frac{1820}{R} \right)^{20} \quad l > 20 \quad (20)$$

which forced the power of the Airy-compensated model to approximately match the observed potential spectrum. Since a downward continuation filter which attenuates the short-wavelength topography is additionally applied to the Bouguer anomaly when computing the crustal structure, the form of the above filter does not significantly affect the crustal thickness results.

We next determine the number of terms in (10) that need to be retained in order to accurately represent the potential due to relief along a density interface. Since (10) is only strictly valid when the observation plane is greater than the maximum relief along this interface, all errors were computed at 8 km above the mean planetary radius. Figure 3 shows the maximum error that is associated with truncating the series at order  $n$ , when compared to the  $n = 10$  solution. Also shown for comparison in this plot is the minimum nearside gravity error of 13.7 mgal.

As can be seen, the complete Bouguer correction is adequately represented by the first two terms. In order to assess how many terms need to be retained when computing the potential for intracrustal relief (upper and lower crustal densities of  $\rho_u = 2800$  and  $\rho_l = 3100 \text{ kg/m}^3$ , respectively), or Moho relief (crustal and mantle densities of  $\rho_c = 2900$  and  $\rho_m = 3400 \text{ kg/m}^3$ , respectively) we have used the first-order version of (18) to obtain an approximation of the relief along these interfaces. Using this relief, the maximum gravity error for the lunar nearside was computed for order  $n$  when compared to the  $n = 10$  solution. In order to obtain the maximum resolution (the maximum model error is less than the minimum lunar gravity error), terms up to  $n = 4$  need to be retained. In the following analysis, all potential anomalies were computed to  $n = 5$ .

After the Bouguer anomaly has been calculated, (18) and (19) or equivalents (see below), were used to calculate the relief along a subsurface density interface. Equation (18) was iterated until the difference between successive gravity solutions was less than  $10^{-4}$  mgal, and the resulting crustal models were constrained to match the seismically determined structure beneath the Apollo 12 and 14 sites [Toksöz *et al.*, 1974; Goins *et al.*, 1981]. Specifically, when intracrustal compensation models were considered, the upper crust was constrained to be 20 km thick at the Apollo 12/14 site, and when compensation at the Moho was

considered, the total crustal thickness was constrained to be 60 km thick at this site.

Since the Bouguer anomaly was filtered in the downward continuation process, the model and observed gravity solutions were not expected to match exactly. Additionally, when taking into account finite amplitude relief along a single density interface, there is no guarantee that a model exists which exactly matches the observed potential. The RMS misfit between the model gravity solutions and the observed GLGM-2 solution were found to be approximately 20 mgal, which is comparable to the formal gravity uncertainties in the GLGM-2 solution ( $\sim 20$  mgal over the equatorial nearside, 30 mgal over the equatorial farside, and 40 mgal over the polar farside). We next present our results for both single- and dual-layered models<sup>1</sup>.

### 3.1. Single Layered Model: Compensation at Moho

The first crustal model that will be considered is one with a uniform density crust and with compensation occurring at the seismically determined lunar Moho. This is the traditional model that was previously considered by Bills and Ferrari [1977], Thurber and Solomon [1978], Bratt *et al.* [1985], Zuber *et al.* [1994], and Neumann *et al.* [1996]. In this model we have used  $\rho_c = 2900 \text{ kg/m}^3$  and  $\rho_m = 3400 \text{ kg/m}^3$ .

Plate 2 shows an image of the crustal thickness minus the mare fill of Plate 1. Crustal thicknesses range from a minimum of  $\sim 13$  km beneath Orientale to a maximum of  $\sim 148$  km on the northeastern rim of the South-Pole Aitken (SPA) basin. The crustal structure of the major basins do not differ significantly from that of Neumann *et al.* [1996] which was derived using a regional higher-order Cartesian algorithm. As has been previously recognized, this model predicts that mantle material should not be exposed at the surface of any of the major impact basins.

Though this model represents a plausible interpretation of the lunar gravity field, as stated in the introduction, there are several geophysical and petrological lines of evidence which suggest that the lunar crust is stratified in some sense. For this reason, the implications of a stratified crust with two layers will be considered in the following models.

### 3.2. Dual Layered Models

**Intracrustal compensation.** The next simplest crustal model is to assume that the crust is stratified and that the entire Bouguer anomaly is due to relief along an intracrustal density interface. This model is consistent with the relationship between the lunar highland geoid to topography ratios [Wieczorek and Phillips, 1997]. For this model we have taken  $\rho_u = 2800 \text{ kg/m}^3$ ,  $\rho_l = 3100 \text{ kg/m}^3$  (see Wieczorek and Phillips [1997] for a discussion of the density of lower crustal material), and Plate 3 shows a plot of the upper crustal thickness minus the mare fill. As can be seen, all of the major nearside basins, as well as SPA basin, have negative crustal thicknesses (by up to 25 km), which is clearly unphysical. Though this model of compensation may be viable for the lunar highlands, relief along the Moho clearly needs to be taken into account when describing the structure of the basins.

<sup>1</sup>Supporting spherical harmonic coefficient files, ASCII raster image files, and FORTRAN program to generate images are available on diskette or via Anonymous FTP from kosmos.agu.org, directory APEND (Username=anonymous, Password=guest). Diskette may be ordered from American Geophysical Union, 2000 Florida Avenue, N.W., Washington, DC 20009 or by phone at 800-966-2481; \$15.00. Payment must accompany order.

**Constant thickness lower crust.** The next model to be considered is a dual-layered crust in which the upper crust is allowed to vary in thickness, while the lower crust has a constant thickness. This model is consistent with the lunar highland geoid to topography ratios [Wieczorek and Phillips, 1997], and (18) and (19) were easily modified to take into account the second layer. The lower crust was constrained to be 40 km thick,  $\rho_u = 2800 \text{ kg/m}^3$ ,  $\rho_l = 3100 \text{ kg/m}^3$ , and  $\rho_m = 3400 \text{ kg/m}^3$ .

The results of this model are shown in Plate 4 where the upper crustal thickness minus mare fill is plotted. This model represents a substantial improvement over the previous model with compensation occurring entirely at an intracrustal interface, but this dual-layered model still has unphysical negative upper crustal thicknesses beneath the basins (by up to 14 km). Though the fit can be improved by altering the Apollo 12/14 reference thickness, as well as by modifying the density contrasts across the intracrustal interface and Moho, for reasonable parameters this model always remains unphysical beneath Crisium basin.

**Upper and lower crustal variations.** The last model to be considered allows both the upper and lower crust to vary in thickness. Since this model is underdetermined, we take an end-member approach and assume that upper crustal thickness variations are the primary cause of the Bouguer anomaly. This is a reasonable assumption since exogenic impact events are the most prominent process which redistribute crustal materials.

In computing the intracrustal and Moho relief, we used the following approach: (1) Using the Bouguer anomaly, the upper crustal thickness was computed assuming that compensation occurred entirely at the intracrustal interface. (2) If the upper crustal thickness was less than zero, the intracrustal relief was modified such that the upper crustal thickness was equal to zero. (3) The potential anomaly due to the modified intracrustal relief was computed and the remainder of the gravity field was explained in terms of relief along the Moho. This approach worked well except north of SPA basin, where the upper crust is extremely thick. In this region, negative lower crustal thicknesses were obtained. To rectify this situation, the upper crustal thickness was reduced in this region and the above procedure was continued at step 3 until the lower crustal thickness was zero.

The upper crustal thickness minus mare fill for this model is shown in Plate 5, and the lower crustal thickness is shown in Plate 6 using  $\rho_u = 2800 \text{ kg/m}^3$ ,  $\rho_l = 3100 \text{ kg/m}^3$ , and  $\rho_m = 3400 \text{ kg/m}^3$ . As can be seen, this model predicts that the entire upper crust has been excavated beneath the major basins and that lower crustal material was additionally excavated beneath many of these basins. Additionally, this model predicts that there should be no lower crustal material to the northeast of SPA basin.

## 4. Discussion

In none of the above models have we considered the possible gravitational contribution of density heterogeneities within the lunar mantle. Though this effect could substantially effect our model results, there are at present no constraints on the location nor magnitude of these postulated anomalies. Without an extensive seismic network, the existence of mantle heterogeneities will remain purely speculative.

Of the four crustal thickness models presented above, only two give physically meaningful results: a single-layered uniform density crust and a dual-layered model with both upper and lower crustal thickness variations. Since there is much evidence which suggests that the lunar crust is vertically stratified, the dual-layered compensation model is our preferred model. In the following

sections we discuss some of the implications of this model for the global structure of the Moon, as well as for the structure of the large impact basins.

### 4.1. Global Structure

This model of lunar structure has an average 31 km thick upper crust and a 29 km thick lower crust (total crustal thickness of 60 km, see Table 1). This is entirely consistent with the model of *Spudis and Davis* [1986], who used geochemical data to infer that the upper half of the crust was anorthositic and that the lower half was noritic in composition. We note also that a 31 km thick upper crust is consistent with it having been formed by the crystallization of a global magma ocean [e.g., *Warren*, 1985].

The degree-1 spherical harmonic coefficients of the crustal thickness maps give an indication of hemispheric differences in the distribution of crustal material. The 1.9 km center-of-mass/center-of-figure offset directed toward 205°E [e.g., *Smith et al.*, 1997] has most often been explained in terms of hemispheric differences in crustal thickness [e.g., *Lingenfelter and Schubert*, 1973; *Haines and Metzger*, 1980], though hemispheric differences in crustal or mantle density are also possible [e.g., *Wasson and Warren*, 1980]. Most recently, assuming a uniform density crust, *Neumann et al.* [1996] have shown that the thickness of the farside crust is approximately 12 km greater than the nearside crust.

Our dual-layered model of crustal structure also predicts that the entire crust is thickened toward the farside but only by about 4 km (see Table 1). The behavior of the upper and lower crustal layers, however, are quite different. The upper crust is significantly thickened toward the farside by 20 km, while the lower crust is thinned toward the farside by 16 km. This dramatic thinning of lower crustal material on the farside is evident in Plate 6 where it is seen that no lower crustal material is present directly north of the South-Pole Aitken basin. If this hemispheric thickness dichotomy is real, and not an artifact of the assumptions that went into the model (namely, the uniform density mantle and crustal layers), two processes may be capable of explaining this feature. *Wood* [1973] has suggested that the Earth may have gravitationally focussed projectiles such that the Moon was asymmetrically bombarded early in its history. Alternatively, *Lingenfelter and Schubert* [1973] have suggested that convective processes may be capable of redistributing large quantities of crustal material. In either case, the gravity and topography data are unable to distinguish between these two hypothesis.

The  $C_{20}$  spherical harmonic coefficient of the crustal thickness maps gives an indication of whether crustal material is concentrated at the poles or equator. Using a single-layered model, *Neumann et al.* [1996] showed that the crust was on average 9.5 km thicker at the equator than at the poles. Our results are similar in that the total crustal thickness is about 5 km thicker at the equator than at the poles. The structure of the upper and lower crust are again quite different, in that the upper crust is about 15 km thicker and the equator, and the lower crust is about 10 km thicker at the poles (see Table 1). If this effect is real, the latitudinal dependence on crustal thickness may be the result of a global magma ocean cooling in the presence of a much faster paleorotation rate.

### 4.2. Impact Basins

The dual-layered model of crustal structure predicts that the entire upper crust was removed beneath the Orientale, Humorum, Imbrium, Serenitatis, Crisium, Nectaris, Smythii, and South-Pole Aitken basins. Additionally, most of these basins show evidence



**Table 1.** Global Properties of Crustal Thickness Models

	Average Crustal Thickness, km	Hemispheric Thickness Difference, km	Direction of Thickened Crust, deg	Equatorial - Polar Thickness, km
<i>Dual-Layered Model:</i>				
Upper crust	30.6	19.8	(3.9 N, -157.6 E)	14.5
Lower crust	29.2	15.8	(3.0 N, 21.2 E)	-9.6
Total crust	59.8	4.0	(7.4 N, -153.0 E)	4.9
<i>Single-Layered Model:</i>				
Total crust	65.9	12.5	(4.4 N, -157.0 E)	11.8

for thinning of the lower crust, suggesting that lower crustal material was also excavated. With the exception of the SPA basin, all of these basins have ejecta blankets that are considerably more noritic than typical highlands material [Spudis *et al.*, 1984, 1996] confirming that lower crustal material was indeed excavated.

It may have been expected that since SPA is the largest known basin on the Moon that mantle material would have been excavated in this event. Somewhat surprisingly, SPA basin has an ~40 km thick lower crust present. Given this considerable thickness of crust in this basin, it appears that mantle material was not excavated. This surprising observation is consistent with spectral reflectance studies of SPA which suggest that the regolith is primarily composed of noritic lower crustal material [Pieters *et al.*, 1997].

It could be argued that since our models do not take into account a possibly large differentiated melt sheet which formed during the SPA basin-forming event, our model does not preclude mantle material from being excavated. As evidence against this interpretation, we note that the iron concentration of the highlands surrounding this basin is surprisingly low and consistent with being composed of upper crustal anorthositic materials. In fact, if the thickened crust north of SPA represents basin ejecta from an oblique impact (as suggested by Zuber *et al.* [1994]), then the extremely low iron concentration of this region suggest that not only was mantle material not excavated, but lower crustal material was not even excavated in this event!

The thinnest crust for our model is found below Crisium basin, in which the total crustal thickness (minus mare fill) is found to be about 5 km. By adjusting the parameters of our model and recognizing that the only crustal thickness constraint is at the Apollo 12 and 14 site, it is possible to model the Crisium basin with a zero crustal thickness. Thus it is possible that the Crisium impact event excavated the entire crustal column, as well as upper mantle material. Given this possibility, it would seem prudent to reanalyze the composition of Crisium's ejecta blanket, as well as material excavated by smaller craters within Crisium, with this prediction in mind. For instance, the high Mg concentrations found in the vicinity of Picard and Pierce craters [Andre *et al.*, 1978] may represent excavated upper mantle material, or an impact melt sheet composed of lower crust and upper mantle material.

Another feature of this model is that there is an annulus of thickened crust (both upper and lower) surrounding most of the major impact basins. This was previously recognized by Neumann *et al.* [1996]. Though the thickened crust surrounding these basins may be real and due to the deposition of basin ejecta and/or related to the excavation flow set up following the impact, it is also possible that it is an artifact of our assumptions about crustal structure. For instance, if the region surrounding the basin was

extensively brecciated or if the ejecta deposits were of a much lower density than the surrounding highland crust, the thickness of these annuli would be decreased [e.g., Phillips and Dvorak, 1981]. Clearly, this is a topic which deserves further study.

## 5. Summary

In this paper we have presented a new technique of analyzing potential anomalies on a sphere due to finite amplitude topography. We have shown that potential anomalies can be computed to arbitrary precision by expanding the topography to the  $n$ th power into spherical harmonics. A filter was also derived which stabilized the process of downward continuing the Bouguer anomaly.

We have used this technique to evaluate several single- and dual-layered crustal thickness models for the Moon, and it was found that only a single-layered model with compensation occurring at the Moho and a dual-layered model with both upper and lower crustal thickness variations gave plausible results. Given that there is much petrologic, seismic, and geophysical evidence which suggests that the crust is stratified, our preferred model is the dual-layered model with upper and lower crustal thickness variations. These crustal thickness maps have many important implications for large-scale global structure, as well as for the large impact basins. Our results suggest that the crust is on average about 60 km thick and that half of this is composed of anorthositic material. In addition, we find that the major nearside basins have excavated the entire upper crust and that lower crustal material was also likely excavated. With the possible exception of Crisium basin, there is no evidence which suggests that mantle material was ever excavated.

**Acknowledgments.** We thank Bruce Bills and Greg Neumann for reviews which improved this paper. This research was supported by NASA grants NAGW-3024 and NAGW-4881.

## References

- Andre, C. G., R. W. Wolfe, and I. Andler, Evidence for a high-magnesium subsurface basalt in Mare Crisium from orbital X-ray fluorescence data, in *Mare Crisium: The View From Luna 24*, edited by R. B. Merrill and J. J. Papike, pp. 1–12, Pergamon Press, Tarrytown, N.Y., 1978.
- Balmino, G., Gravitational potential harmonics from the shape of an homogeneous body, *Celestial Mech. Dyn. Astron.*, **60**, 331–364, 1994.
- Bills, B. G., and A. J. Ferrari, A lunar density model consistent with topographic, gravitational, librational, and seismic data, *J. Geophys. Res.*, **82**, 1306–1314, 1977.
- Bratt, S. R., S. C. Solomon, J. W. Head, and C. F. Thurber, The deep structure of lunar basins: Implications for basin formation and modification, *J. Geophys. Res.*, **90**, 3049–3064, 1985.
- Charette, M. P., S. R. Taylor, J. B. Adams, and T. B. McCord, The detection of soils of Fra Mauro basalt and anorthositic gabbro composition in the lunar highlands by remote spectral reflectance techniques, *Proc. Lunar Sci. Conf.*, **8th**, 1049–1061, 1977.

- DeHon, R. A., Thickness of the western mare basalts, *Proc. Lunar Planet. Sci. Conf.*, 10th, 2935–2955, 1979.
- DeHon, R. A., and J. D. Waskom, Geologic structure of the eastern mare basins, *Proc. Lunar Sci. Conf.*, 7th, 2729–2746, 1976.
- Dorman, L. M., and T. R. Lewis, Experimental isostasy, 1, Theory of the determination of the Earth's isostatic response to a concentrated load, *J. Geophys. Res.*, 75, 3357–3365, 1970.
- Goins, N. R., A. M. Dainty, and M. N. Toksöz, Lunar seismology: The internal structure of the Moon, *J. Geophys. Res.*, 86, 5061–5074, 1981.
- Haines, E. L., and A. E. Metzger, Lunar highland crustal models based on iron concentrations: Isostasy and center-of mass displacement, *Proc. Lunar Planet. Sci. Conf.*, 11th, 689–718, 1980.
- Kaula, W. M., Theory of statistical analysis of data distributed over a sphere, *Rev. Geophys.*, 5, 83–107, 1967.
- Lambeck, K., *Geophysical Geodesy: The Slow Deformation of the Earth*, Clarendon Press, Oxford, England, 1988.
- Lemoine, F. G., D. E. Smith, M. T. Zuber, G. A. Neumann, and D. D. Rowlands, A 70th degree lunar gravity model (GLGM-2) from Clementine and other tracking data, *J. Geophys. Res.*, 102, 16,339–16,359, 1997.
- Lingenfelter, R. E., and G. Schubert, Evidence for convection on planetary interiors from first order topography, *Moon*, 7, 172–180, 1973.
- Neumann, G. A., M. T. Zuber, D. E. Smith, and F. G. Lemoine, The lunar crust: Global structure and signature of major basins, *J. Geophys. Res.*, 101, 16,841–16,843, 1996.
- Nozette, S., et al., The Clementine mission to the Moon: Scientific overview, *Science*, 266, 1835–1839, 1994.
- Oldenburg, D. W., The inversion and interpretation of gravity anomalies, *Geophysics*, 39, 526–536, 1974.
- Parker, R. L., The rapid calculation of potential anomalies, *Geophys. J. R. Astron. Soc.*, 31, 447–455, 1972.
- Parker, R. L., and S. P. Huestis, The inversion of magnetic anomalies in the presence of topography, *J. Geophys. Res.*, 79, 1587–1593, 1974.
- Phillips, R. J., and J. Dvorak, The origin of lunar mascons: Analysis of the Bouguer gravity associated with Grimaldi, in *Multi-ring Basins*, edited by P. H. Schultz and R. B. Merrill, *Proc. Lunar Planet. Sci.*, 12A, 91–104, 1981.
- Phipps Morgan, J., and D. K. Blackman, Inversion of combined gravity and bathymetry data for crustal structure: A prescription for downward continuation, *Earth Planet. Sci. Lett.*, 119, 167–179, 1993.
- Pieters, C. M., S. Tompkins, J. W. Head, and P. C. Hess, Mineralogy of the mafic anomaly in the South Pole-Aitken basin: Implications for excavation of the lunar mantle, *Geophys. Res. Lett.*, 24, 1903–1906, 1997.
- Rapp, R. H., The decay of the spectrum of the gravitational potential and the topography of the Earth, *Geophys. J. Int.*, 99, 449–455, 1989.
- Ryder, G., and J. A. Wood, Serenitatis and Imbrium impact melts: Implications for large-scale layering in the lunar crust, *Proc. Lunar Sci. Conf.*, 8th, 655–668, 1977.
- Smith, D. E., M. T. Zuber, G. A. Neumann, and F. G. Lemoine, Topography of the Moon from Clementine lidar, *J. Geophys. Res.*, 102, 1591–1611, 1997.
- Solomon, S. C., and J. W. Head, Lunar mascon basins: Lava filling, tectonics, and evolution of the lithosphere, *Rev. Geophys.*, 18, 107–141, 1980.
- Spudis, P. D., and P. A. Davis, A chemical and petrological model of the lunar crust and implications for lunar crustal origin, *Proc. Lunar Planet. Sci. Conf.*, 17th, Part 1, *J. Geophys. Res.*, 91, suppl., E84–E90, 1986.
- Spudis, P. D., B. R. Hawke, and P. Lucey, Composition of Orientale basin deposits and implications for the lunar basin-forming process, *Proc. Lunar Planet. Sci. Conf.*, 15th, Part 1, *J. Geophys. Res.*, 89, suppl., C197–C210, 1984.
- Spudis, P. D., B. R. Hawke, P. G. Lucey, G. J. Taylor, and K. Stockstill, Composition of the ejecta deposits of selected lunar basins from Clementine elemental maps (abstract), *Lunar Planet. Sci. XXVII*, 1255–1256, 1996.
- Thurber, C. H., and S. C. Solomon, An assessment of crustal thickness variations on the lunar near side: Models, uncertainties, and implications for crustal differentiation, *Proc. Lunar Planet. Sci. Conf.*, 9th, 3481–3497, 1978.
- Toksöz, M. N., A. M. Dainty, S. C. Solomon, and K. R. Anderson, Structure of the Moon, *Rev. Geophys.*, 12, 539–567, 1974.
- Varshalovich, D. A., A. N. Moskalov, and V. K. Khersonskii, *Quantum Theory of Angular Momentum*, World Sci., Singapore, 1988.
- Warren, P. H., The magma ocean concept and lunar evolution, *Annu. Rev. Earth Planet. Sci.*, 13, 201–240, 1985.
- Wasson, J. T., and P. H. Warren, Contribution of the mantle to the lunar asymmetry, *Icarus*, 44, 752–771, 1980.
- Wieczorek, M. A., and R. J. Phillips, The structure and compensation of the lunar highland crust, *J. Geophys. Res.*, 102, 10,933–10,943, 1997.
- Williams, K. K., and M. T. Zuber, Re-evaluation of mare thicknesses based on lunar crater depth-diameter relationships (abstract), *Lunar Planet. Sci.*, XXVII, 1441–1442, 1996.
- Wood, J. A., Bombardment as a cause of the lunar asymmetry, *Moon*, 8, 73–103, 1973.
- Zuber, M. T., D. E. Smith, F. G. Lemoine, and G. A. Neumann, The shape and internal structure of the Moon from the Clementine mission, *Science*, 266, 1839–1843, 1994.

R. J. Phillips and M. A. Wieczorek, Department of Earth and Planetary Sciences, Washington University, Box 1169, One Brookings Drive, St. Louis, MO 63130. (e-mail: phillips@wustite.wustl.edu; markw@wurtzite.wustl.edu)

(Received July 9, 1997; revised October 23, 1997; accepted October 30, 1997.)